

MPI-PhE/2001-13
July 2001

STANDARD MODEL PHYSICS AT HERA

Vladimir Chekelian (Shekelyan)
MPI für Physik (Munich) and ITEP (Moscow)
(on behalf of the H1 and ZEUS Collaborations)

Abstract

Both components of the Standard Model, QCD and the electroweak sector, are tested in the H1 and ZEUS experiments at HERA. The inclusive e^-p and e^+p single and double differential cross sections for neutral and charged current processes are measured in the range of four-momentum transfer squared, Q^2 , between 0.045 and 30 000 GeV^2 , and Bjorken x between 10^{-6} and 0.65. The neutral current double differential cross section, from which the proton structure function $F_2(x, Q^2)$ and the longitudinal structure function $F_L(x, Q^2)$ are extracted, is measured at low x with typically 1% statistical and 2-3% systematic uncertainties. In a next-to-leading order (NLO) DGLAP QCD analysis using the H1 measurements and the μp data of the BCDMS collaboration the strong coupling constant α_s and the gluon momentum distribution are simultaneously determined. A value of $\alpha_s(M_Z^2) = 0.1150 \pm 0.0017(\text{exp})_{-0.0005}^{+0.0009}(\text{model})$ is obtained, with an additional theoretical uncertainty of about ± 0.005 , mainly due to the uncertainty of the renormalisation scale. F_2^c , the charm contribution to F_2 , is measured and well described by the boson gluon fusion production mechanism using the gluon distribution from the NLO QCD analysis. The gluon distribution and the strong coupling constant α_s are also determined from jet production. For $Q^2 > 1\,000\,\text{GeV}^2$, an asymmetry between e^+p and e^-p neutral current scattering is observed and the structure function xF_3 is extracted. A fit to the charged current data is used to determine a value for the W boson propagator mass. All data are found to be in good agreement with Standard Model predictions.

*Talk given at XV Rencontres de Physique de la Vallée d'Aoste, La Thuile, Italy,
March 4-10, 2001*

1 Introduction

An understanding of the structure of the proton in terms of partons, i.e. quarks and gluons which follow QCD dynamics, was established to a large extent in lepton-proton, in particular electron-proton, deep inelastic scattering (DIS). At the HERA ep collider with an electron-proton centre-of-mass energy of $\sqrt{s}=320$ GeV, effects of the electroweak sector can also be tested in DIS in the region where the squared four momentum transfer $Q^2 \simeq M_Z^2$ or M_W^2 (M_Z and M_W are the Z^0 and W boson masses). In addition, signals of new physics beyond the Standard Model may be expected to arise at the highest Q^2 where the proton structure is probed at smallest distances.

Deep inelastic scattering, Fig. 1, depends on three variables, Q^2 , x and y , where $Q^2 = -q^2$ and $x = Q^2/2(Pq)$ is the fraction of the proton momentum carried by the struck quark and $y = (Pq)/(Pk)$ is the inelasticity of the interaction. The variables are related via $Q^2 = sxy$.

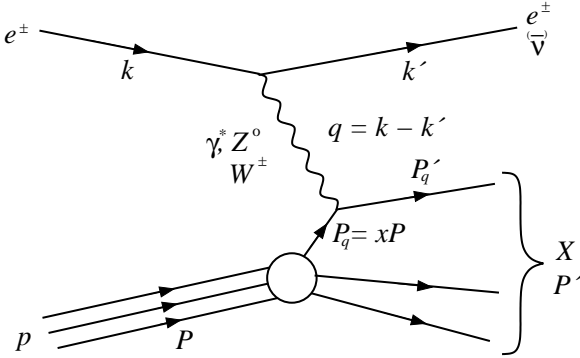


Figure 1: *Feynman diagram for deep inelastic scattering (DIS). The kinematics is defined by the four-vectors of the incoming proton, P , the incoming electron, k , the scattered electron, k' , and the exchanged boson, $q = k - k'$.*

The electron-proton neutral current (NC) and charged current (CC) cross sections can each be expressed in terms of three proton structure functions. For neutral current interactions mediated by a γ or Z^0 boson, the proton structure function $F_2(x, Q^2)$ dominates the cross section and is proportional to the sum of the quark momentum distributions weighted by the quark charge squared. The longitudinal structure function $F_L(x, Q^2)$ is directly sensitive to the gluon momentum distribution. The structure function $x F_3(x, Q^2)$ is related to valence quarks only. These three proton structure functions have been measured at HERA and confronted with the Standard Model predictions. The gluon momentum distribution and the strong coupling α_s determined in a QCD analysis of the HERA inclusive data have been cross checked in more exclusive channels such as charm and jet production via boson gluon fusion. The propagator mass M_W has been determined from the Q^2 dependence of the CC interactions and can be compared with direct M_W mass

measurements in e^+e^- and $p\bar{p}$ interactions. Thus, measurements at HERA provide tests of both components of the theory, the electroweak sector and the evolution of the parton densities as predicted by perturbative QCD.

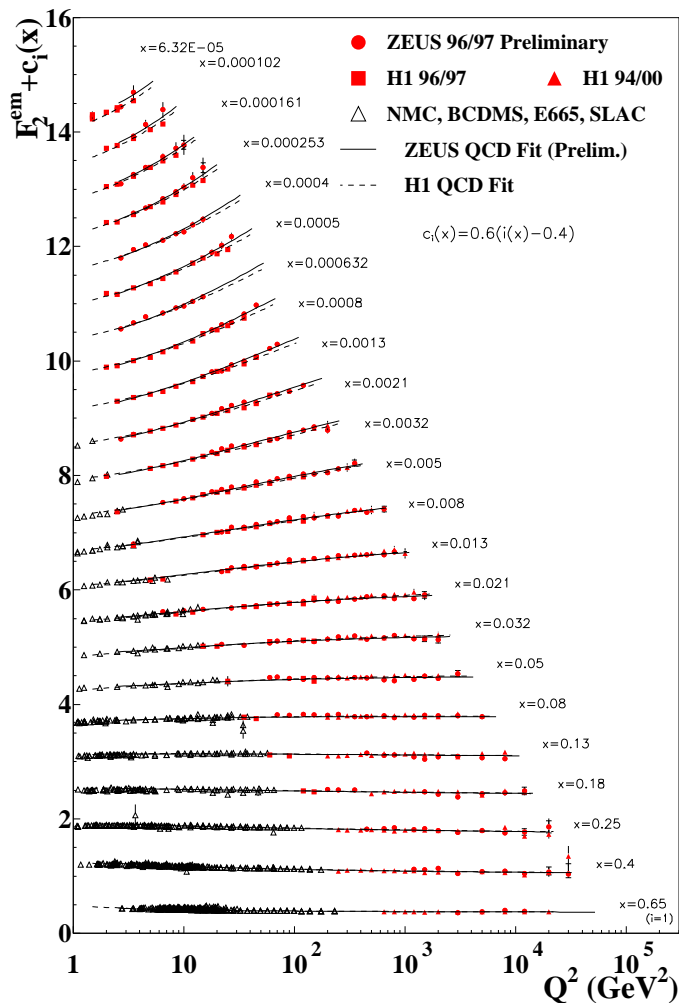


Figure 2: *Measurement of the proton structure function $F_2(x, Q^2)$ by H1 and ZEUS and by fixed target charged lepton-proton experiments. The H1 and ZEUS NLO QCD fits are also shown.*

2 Results

The first F_2 measurements ¹⁾ in ep interactions at HERA, based on a luminosity of 0.025 pb^{-1} collected in 1992, revealed at low x a pronounced rise of F_2 with decreasing x which generated a new interest in QCD in DIS. Since then the collected luminosity has been increased by more than three orders of magnitude. In addition, the H1 and ZEUS detectors have been continuously improved. In 1995/1996 new detector components were installed by H1: the backward calorimeter Spacal, the backward drift chamber BDC and the backward silicon tracker BST. In 1995 the

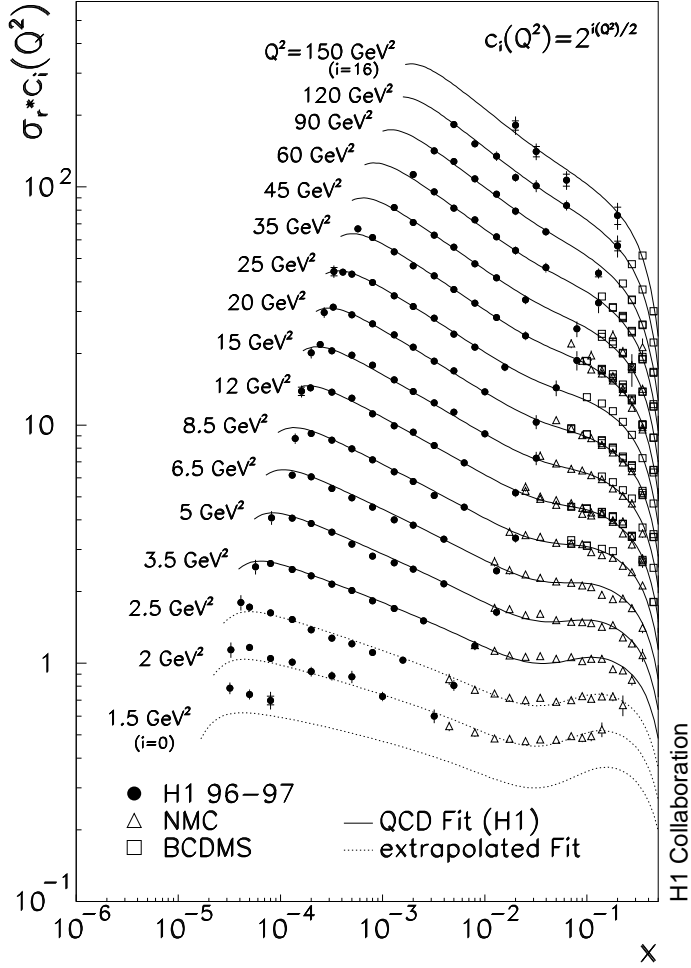


Figure 3: *Measurement of the NC reduced cross section. The solid curves show the result of a QCD fit to the H1 data with $Q^2 \geq 3.5 \text{ GeV}^2$. The dashed curves show the extrapolation of this fit towards lower Q^2 .*

ZEUS collaboration installed a beam pipe calorimeter (BPC) and in 1997 a beam pipe tracker (BPT) was added, covering very small angles of the scattered electron. These improvements and the increase in luminosity made it possible to extend the measured region ^{2, 3, 4, 5)} to very low $Q^2 \geq 0.045 \text{ GeV}^2$, covering the transition region from DIS to real photoproduction ($Q^2 = 0$), as well as very high $Q^2 \geq 10^4 \text{ GeV}^2$. The variable x ranges from 10^{-6} to 0.65 in the valence quark region. F_2 measurements ^{6, 7)} at HERA together with fixed target experiments are shown in Fig. 2 as a function of Q^2 for different values of x . The H1 and ZEUS data agree very well in the full range accessible by the HERA experiments. At very low $y = 0.003$, the HERA data overlap and agree with the data of the fixed target experiments. In a large part of the phase space the precision of the data is 2–3% which is comparable with that of fixed target experiments.

The results on the reduced NC cross section, defined as the cross section divided by the kinematical factor $(2\pi\alpha^2 Y_+)/ (Q^4 x)$ with $Y_+ = 1 + (1 - y)^2$ and α , the

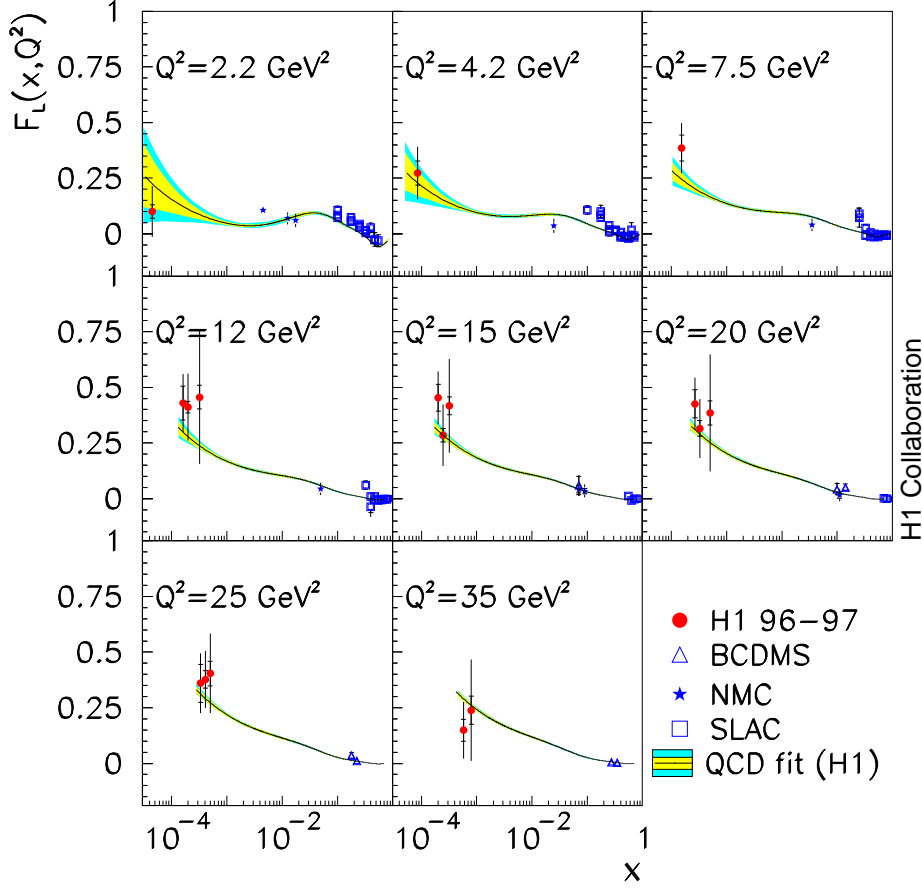


Figure 4: The longitudinal structure function $F_L(x, Q^2)$ for different bins of Q^2 as obtained by H1 at low x , and by charged lepton-nucleon fixed target experiments at large x . The outer (inner) error bars show the total (statistical) errors. The error bands are due to the experimental (inner) and model (outer) uncertainty of the calculation of F_L using the QCD fit to the H1 data for $y < 0.35$ and $Q^2 \geq 3.5 \text{ GeV}^2$.

fine structure constant, are shown in Fig. 3 as function of x for $1.5 \leq Q^2 \leq 150 \text{ GeV}^2$. At very high y ($y \simeq 0.82$), i.e. the lowest x points at fixed Q^2 , a turn over is visible in the measured cross section which is due to the longitudinal structure function $F_L(x, Q^2)$. From these high- y cross sections, $F_L(x, Q^2)$ was extracted ⁶⁾ as shown in Fig. 4. This extends the knowledge of the longitudinal structure function to much lower x than available from fixed target lepton-proton scattering experiments. The increase of $F_L(x, Q^2)$ towards low x is consistent with the QCD calculation, reflecting the rise of the gluon momentum distribution towards low x .

Another quantity related to the gluon density is the derivative $(\partial F_2 / \partial \ln Q^2)_x$ which is shown as a function of x in Fig. 5a, b for different Q^2 . The derivatives show

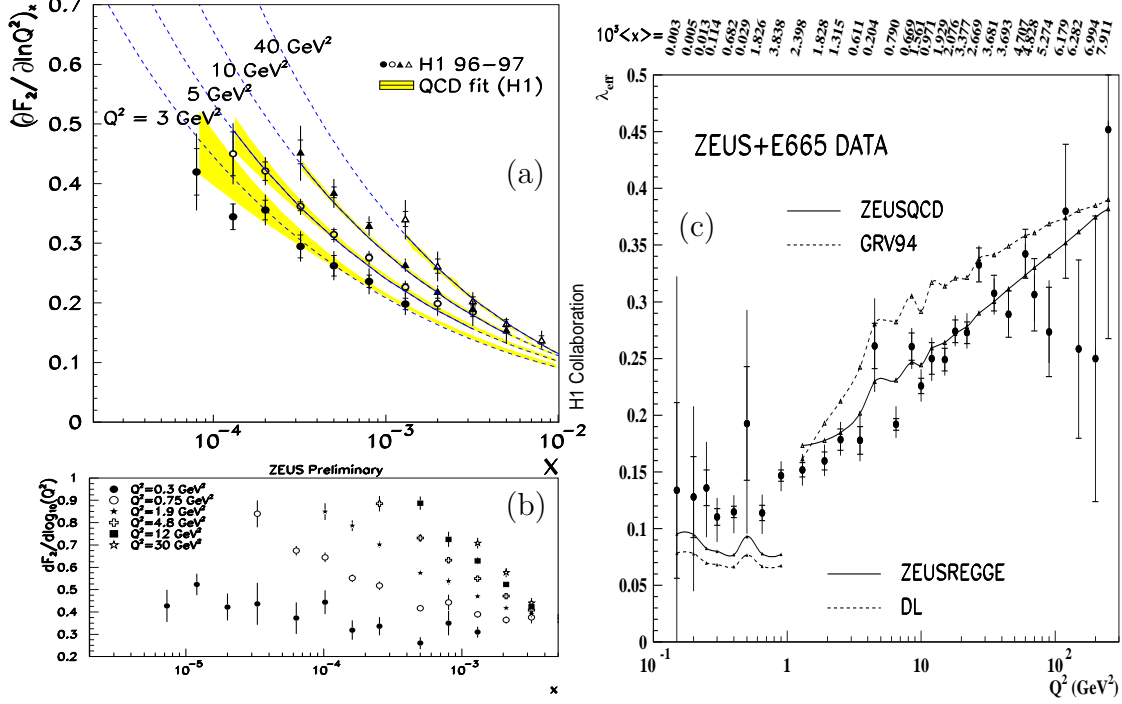


Figure 5: (a),(b) The derivative $(\partial F_2 / \partial \ln Q^2)_x$ plotted as functions of x for different Q^2 , for the H1 and ZEUS data (symbols). The QCD fit to the H1 data for $Q^2 \geq 3.5 \text{ GeV}^2$ is shown by solid lines. The dashed curves extrapolate this fit. The error bands represent the model uncertainty of the QCD analysis. (c) $\lambda_{eff} = d \ln F_2 / d \ln(1/x)$ as a function of Q^2 calculated by fitting $F_2 = A x^{-\lambda_{eff}}$ to ZEUS and E665 data with $x < 0.01$. The inner error bar shows the statistical error and the outer the total statistical and systematic error added in quadrature.

a continuous rise towards low x for fixed Q^2 which is well described by the QCD fit to the H1 data down to $Q^2 = 3 \text{ GeV}^2$. The shape of $(\partial F_2 / \partial \ln Q^2)_x$ reflects the behaviour of the gluon distribution in the associated kinematic range.

The rise of F_2 with decreasing x can be characterised by $F_2 \propto x^{-\lambda_{eff}}$ where $\lambda_{eff} = d \ln F_2 / d \ln(1/x)$. In Fig. 5c, values of λ_{eff} are shown from fits at fixed Q^2 to the F_2 data. The prominent rise of F_2 at large Q^2 values is in agreement with the QCD fit⁸⁾. For smaller Q^2 , the rise of F_2 becomes less steep and λ_{eff} approaches a value of ≈ 0.08 expected from the Regge motivated fits^{8, 9)}.

The high precision of the data allows a simultaneous determination of the gluon distribution and the strong coupling constant α_s in a next-to-leading-order (NLO) DGLAP¹⁰⁾ QCD fit⁶⁾ by combining the low x cross section data of H1 with μp scattering data of the BCDMS collaboration¹¹⁾ at large x . The gluon

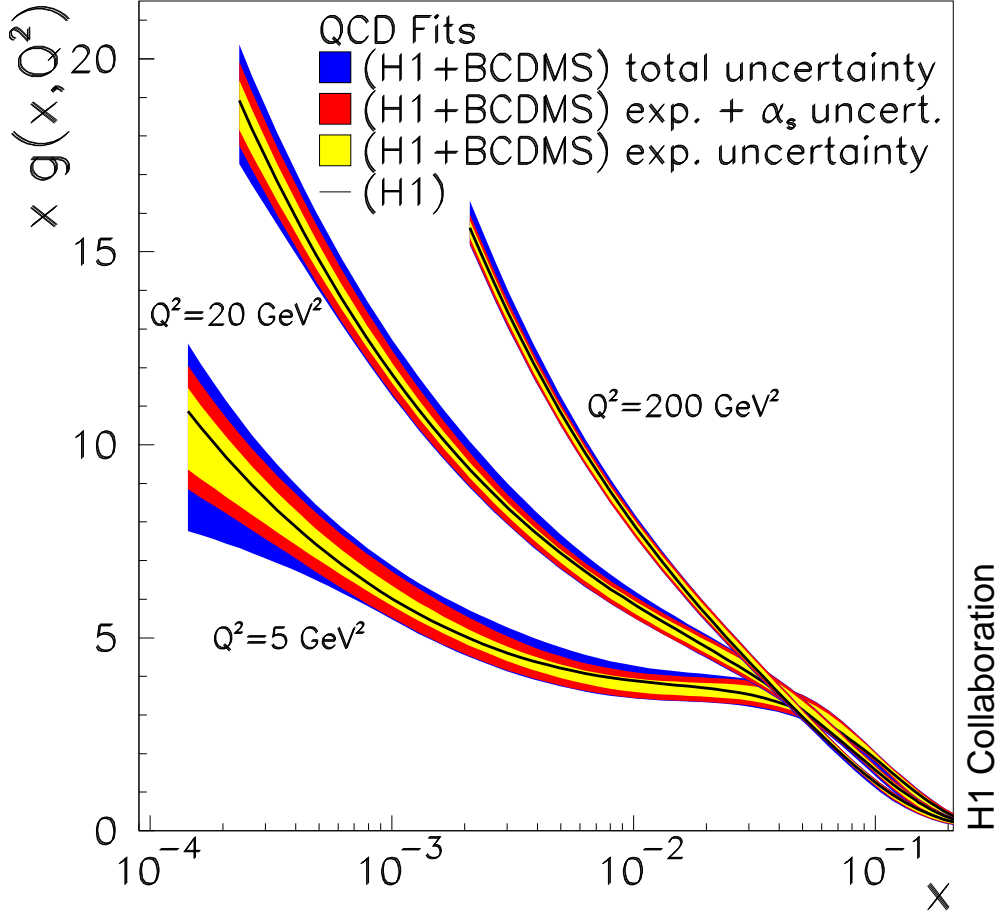


Figure 6: *Gluon distribution resulting from the QCD fit to H1 ep and BCDMS μp data. The innermost error bands represent the experimental error for fixed $\alpha_s(M_Z^2)=0.1150$. The middle error bands include in addition the contribution due to the simultaneous fit of α_s . The outer error bands also include the model uncertainties of the QCD analysis and the dependence on the data range fitted.*

distribution from this fit is shown in Fig. 6 for $Q^2=5, 20$, and 200 GeV^2 . The inner error band represents the experimental uncertainty of the determination of xg for α_s fixed. The simultaneous determination of $xg(x, Q^2)$ and α_s leads to a small increase of the experimental error of xg as is illustrated by the middle error band. The full error band includes in addition the uncertainties connected with the fit ansatz (“model uncertainty”). The DGLAP analysis of the data leads to a gluon distribution which rises dramatically at small x with increasing Q^2 . A value of the strong coupling constant $\alpha_s(M_Z^2) = 0.1150 \pm 0.0017(\text{exp}) \pm_{0.0005}^{0.0009}(\text{model})$ is obtained. The value of α_s changes by about 0.005, much more than the experimental error, if the renormalisation scale is allowed to vary by a factor of four in the fit. This

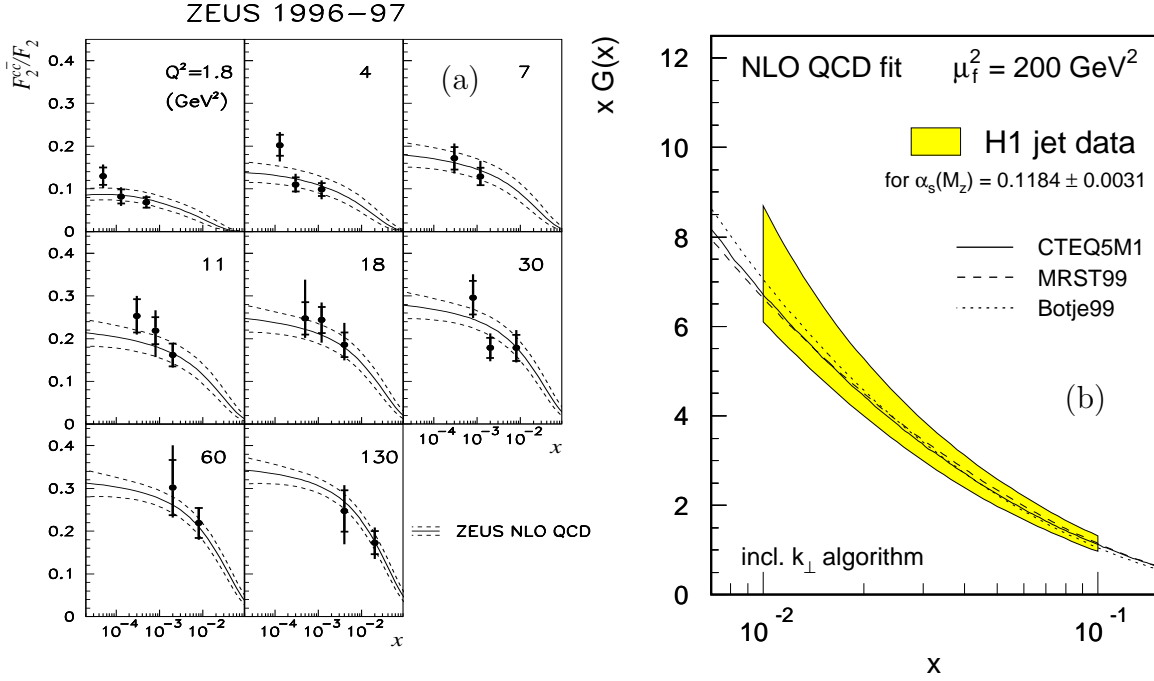


Figure 7: Charm contribution to F_2 in comparison with calculations using the NLO QCD fit to F_2 (a). Gluon distribution resulting from jet studies (b). The error band includes the experimental and the theoretical uncertainties as well as the uncertainty of $\alpha_s(M_Z^2)$.

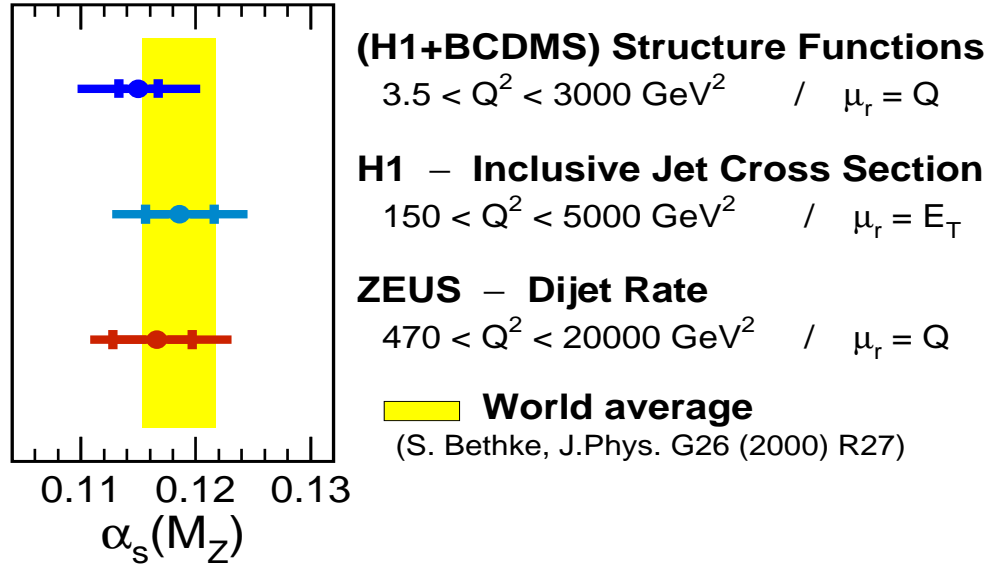


Figure 8: Measurements of the strong coupling constant $\alpha_s(M_Z^2)$ at HERA in comparison with the world average. Inner error bars represent experimental errors, outer error bars represent total errors including the theoretical uncertainty mainly due to the uncertainty of the renormalisation and the factorisation scales.

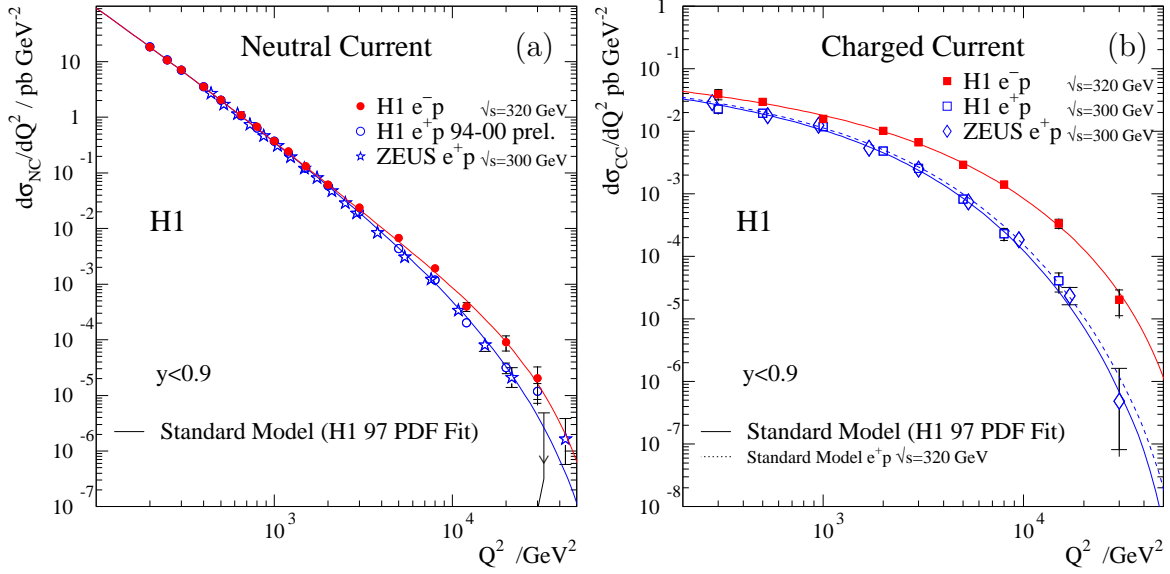


Figure 9: The Q^2 dependences of the NC (a) and CC (b) cross sections are shown for the e^-p (solid symbols) and e^+p data (open symbols). The data are compared with the Standard Model expectations determined from the NLO QCD fit.

theoretical uncertainty is expected to be reduced significantly in next-to-next-to-leading-order (NNLO) perturbation theory.

Exclusive channels such as charm or jet production via boson gluon fusion can also be used for a direct extraction of the gluon density. The charm contribution to F_2 , F_2^c , is determined at HERA using measurements of D^* production and account for 25 – 30% of F_2 ¹²⁾ as shown in Fig. 7a. The F_2^c results are in agreement with expectations calculated using the gluon momentum distribution as determined in the NLO QCD fit to the inclusive cross sections. Jet production data ¹³⁾ could be used to determine the gluon distribution using α_s from other experiments, or determine the strong coupling constant α_s using parton momentum distributions from global QCD fits. The resulting gluon distribution at the factorisation scale $\mu_f = \sqrt{200}$ GeV is shown in Fig. 7b and consistent with the gluon from the global QCD fits. The results for α_s from jet studies by H1 and ZEUS collaborations together with α_s determined from scaling violations by H1 are shown in Fig. 8 in comparison with the world average ¹⁴⁾.

Purely electroweak effects become observable at HERA in a region of very high Q^2 comparable with the masses squared of the vector bosons Z^0 and W . Especially interesting in this respect is the comparison of neutral and charged current

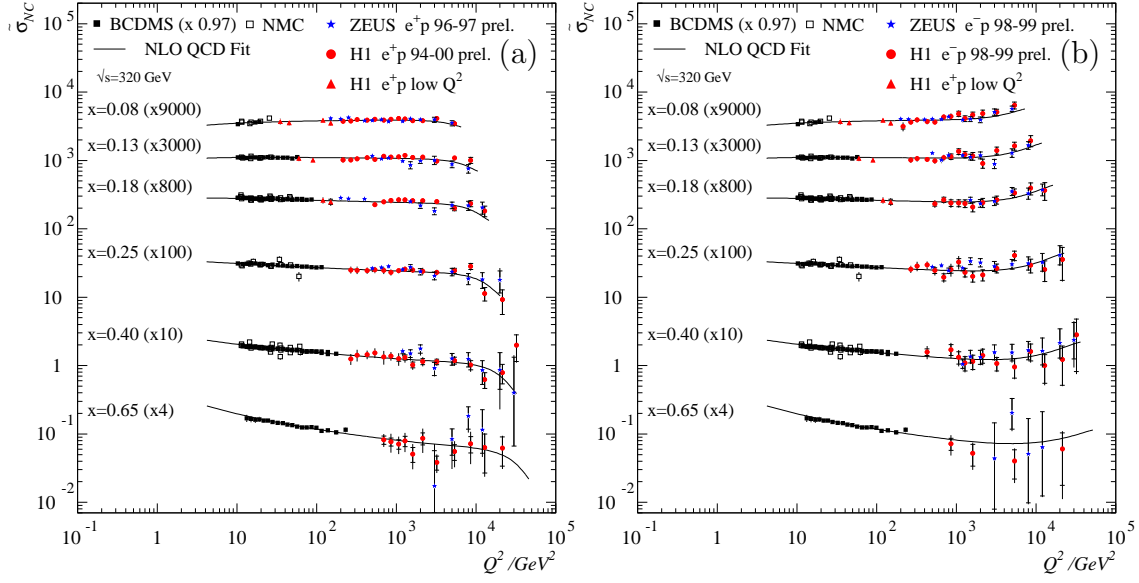


Figure 10: The NC e^+p (a) and e^-p (b) reduced cross sections are shown at high x together with fixed target data from BCDMS and NMC. The curves represent the Standard Model expectation based on the NLO QCD Fit.

cross sections 4, 5, 15, 16, 17) shown in Fig. 9. At low Q^2 , the cross section of the CC process, which is due to exchange of the W boson, is suppressed compared to that of the NC process due to the different propagator terms. At high $Q^2 \approx M_W^2$, both cross sections are approaching each other manifesting the unification of the weak and electromagnetic forces.

Electroweak effects are also visible in the comparison of the e^-p and e^+p NC cross sections. Due to Z^0 exchange, at very high Q^2 the NC cross section is predicted to be suppressed in e^+p and enhanced in e^-p interactions. This effect becomes visible for $Q^2 \geq 1000 \text{ GeV}^2$ as shown in Fig. 9a, 10 and agrees with the Standard Model prediction.

The difference of the NC e^+p and e^-p cross sections at large Q^2 has been used to extract the structure function xF_3 in the range $0.02 < x < 0.65$ and $1500 \leq Q^2 \leq 30000 \text{ GeV}^2$ as shown in Fig. 11. Since at HERA the dominant contribution to xF_3 is due to photon- Z^0 interference, the H1 collaboration evaluated the corresponding structure function $xF_3^{\gamma Z}$. The result is shown in Fig. 12. The integral $\int_{0.02}^{0.65} F_3^{\gamma Z} dx = 1.88 \pm 0.35(\text{stat.}) \pm 0.27(\text{syst.})$ is found to be consistent within experimental errors with theoretical expectation of 1.11 [15].

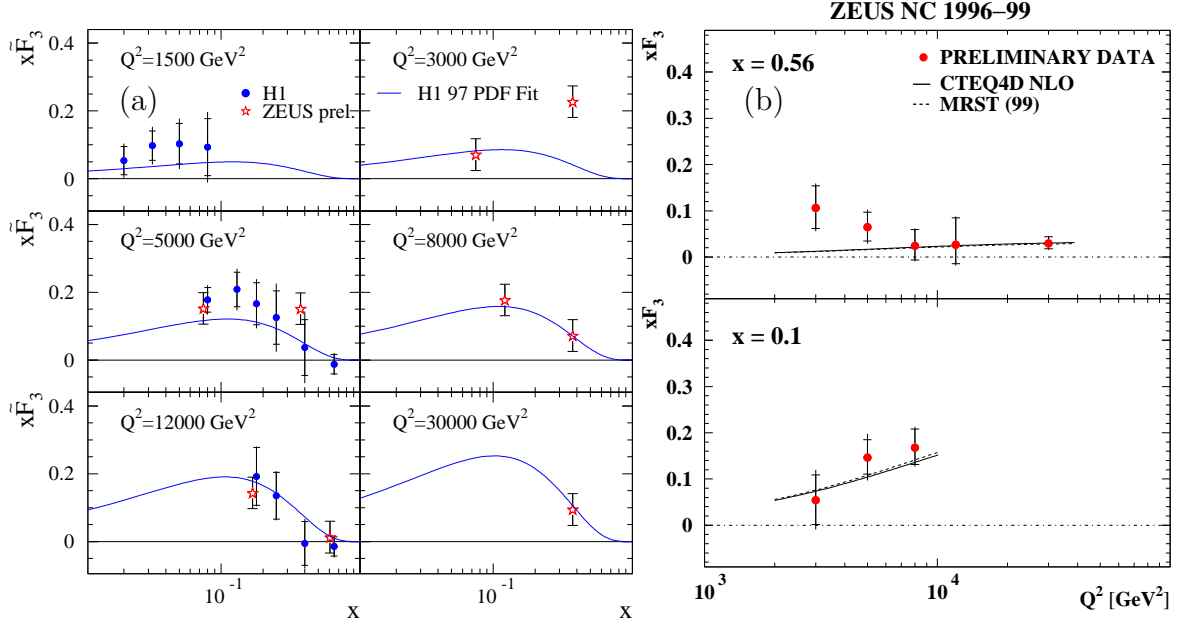


Figure 11: The structure function xF_3 measured by H1 and ZEUS is compared with the H1 97 PDF Fit ⁴⁾ and global fits ^{18, 19)}.

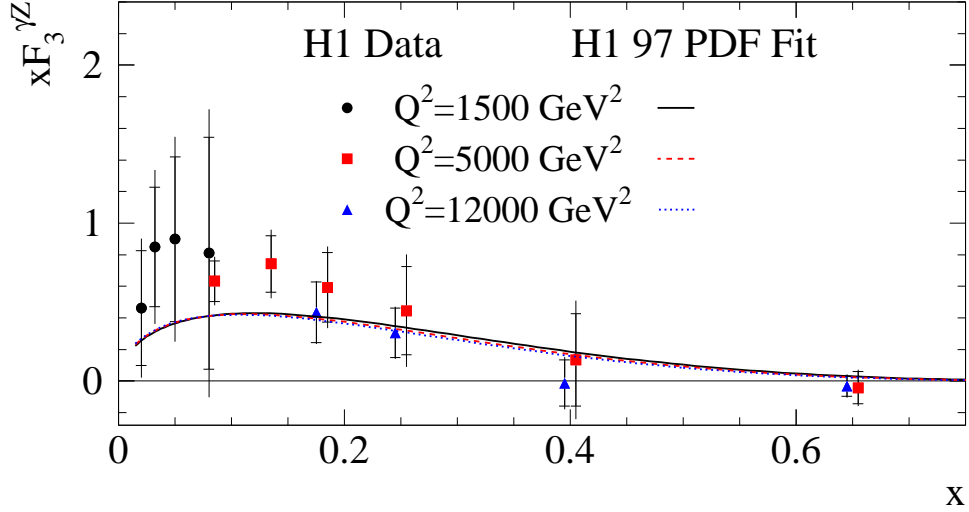


Figure 12: The structure function $xF_3^{\gamma Z}$ measured by the H1 collaboration is compared with the H1 97 PDF Fit ⁴⁾.

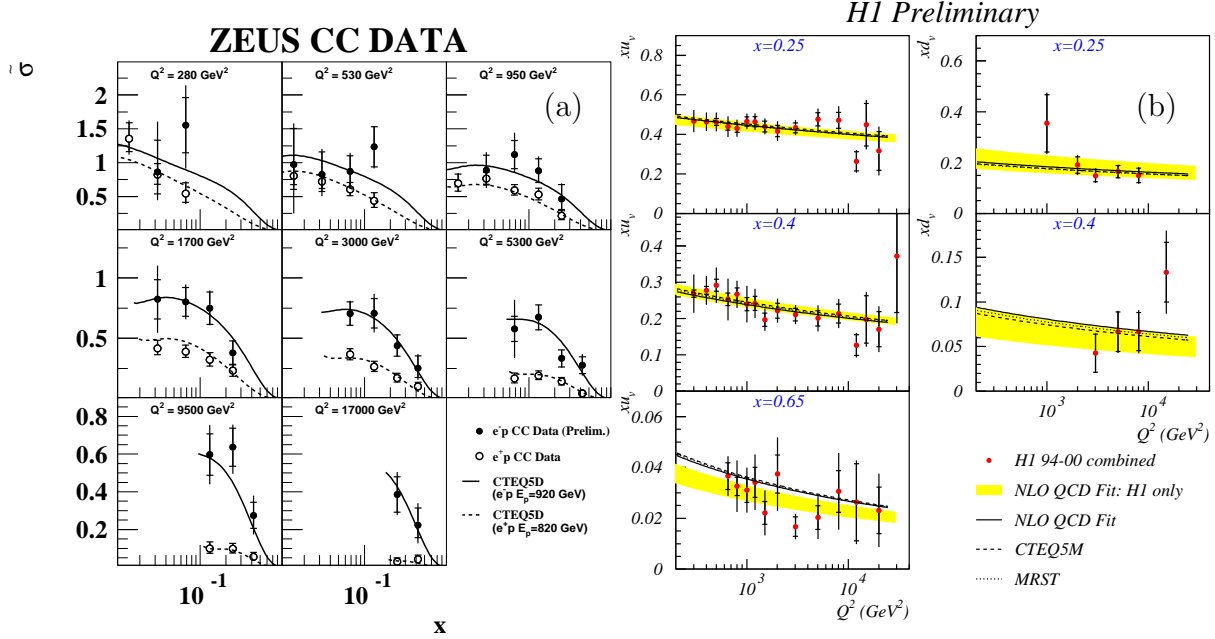


Figure 13: The CC e^\pm reduced cross sections are compared with global QCD fit (a). The valence quarks distributions xu_v and xd_v determined using a local extraction method in comparison with the H1 NLO QCD and global fits ^{18, 19} (b).

The reduced CC cross sections, defined in analogy to the NC case as the cross section divided by $(G_F^2 M_W^4)/(2\pi x(M_W^2 + Q^2)^2)$ with the Fermi coupling constant G_F , are shown in Fig. 13a. The results are well described by the Standard Model expectations. At high x the e^-p and e^+p cross sections are dominated by the valence quark contributions, xu_v and $(1-y)^2 xd_v$ respectively. For points where the expected xq_v contribution to the total cross section is larger than 70% a local extraction method ¹⁷⁾ is used to determine the valence quark densities:

$$xq_v(x, Q^2) = \sigma_{meas}(x, Q^2) \left(\frac{xq_v(x, Q^2)}{\sigma(x, Q^2)} \right)_{theory}$$

where σ_{meas} is the measured NC or CC $e^\pm p$ double differential cross sections and the ratio is the theoretical expectation from the H1 97 PDF Fit ⁴⁾. The extracted parton densities shown in Fig. 13b are rather independent of the theoretical input and are in agreement with global fits.

Within the Standard Model, CC interactions are mediated by the t -channel exchange of a W boson, and therefore are sensitive to the W mass in the space-like regime. The propagator mass M_W is fitted to the double differential CC cross section

data and yields for e^+p and e^-p respectively 5, 15)

$$M_W = 81.4_{-2.6}^{+2.7}(\text{stat.}) \pm 2.0(\text{syst.})_{-3.0}^{+3.3}(\text{th.}) \text{ GeV}$$

$$M_W = 79.9 \pm 2.2(\text{stat.}) \pm 0.9(\text{syst.}) \pm 2.1(\text{th.}) \text{ GeV}$$

These values are consistent with direct measurements in the time-like domain from LEP and TEVATRON.

3 Conclusions

The present tests of the Standard Model show good agreement of predictions of perturbative QCD and electroweak theory with the HERA data. The luminosity upgrade of the HERA collider will bring the opportunity to improve the precision of such tests, especially for the electroweak sector at high Q^2 where the precision of the measurements is still limited by statistics.

References

1. H1 Collab., I. Abt et al., Nucl.Phys. B407 (1993) 515;
ZEUS Collab., M. Derrick et al., Phys. Lett. B316 (1993) 412.
2. H1 Collab., S. Aid et al., Nucl. Phys. B470 (1996) 3;
H1 Collab., S. Aid et al., Phys. Lett. B393 (1997) 452;
H1 Collab., C. Adloff et al., Nucl. Phys. B497 (1997) 3.
3. ZEUS Collab., M. Derrick et al., Zeitschrift f. Physik C72 (1996) 399;
ZEUS Collab., J. Breitweg et al., Phys. Lett. B487 (2000) 53.
4. H1 Collab., C. Adloff et al., Eur. Phys. J. C13 (2000) 609.
5. ZEUS Collab., J. Breitweg et al., Eur. Phys. J. C11 (1999) 427;
ZEUS Collab., J. Breitweg et al., Eur. Phys. J. C12 (2000) 411.
6. H1 Collab., C. Adloff et al., Deep-Inelastic Inclusive ep Scattering at Low x and a Determination of α_s , DESY-00-181, hep-ex/0012053, accepted by Eur.Phys.J.C.
7. ZEUS Collab., Measurement of the Proton Structure Function F_2 in e^+p Collisions at HERA, contrubuted paper to ICHEP 2000, Osaka, Japan, July 2000.
8. ZEUS Collab., J. Breitweg et al.,Eur. Phys. J. C7 (1999) 609.
9. A. Donnachie and P. V. Landshoff, Z. Phys. C61 (1994) 139.

10. Yu. L. Dokshitzer, Sov. Phys. JETP 46 (1977) 641;
V. N. Gribov and L. N. Lipatov, Sov. J. Nucl. Phys. 15 (1972) 438 and 675;
G. Altarelli and G. Parisi, Nucl. Phys. B126 (1977) 298.
11. BCDMS Collaboration, A.C. Benvenuti et al., Phys. Lett. B223 (1989) 485;
CERN preprint CERN-EP/89-06.
12. H1 Collab., C. Adloff et al., Measurement of D^* Meson Production and the Charm Contribution to the Proton Structure F_2^c in Deep Inelastic Scattering at HERA, contributed paper to ICHEP 2000, Osaka, Japan, July 2000;
ZEUS Collab.; J. Breitweg et al., Eur. Phys. J. C12 (2000) 35.
13. H1 Collab., C. Adloff et al., Eur. Phys. J. C19 (2001) 289;
ZEUS Collab., J. Breitweg et al., Phys. Lett. B507 (2001) 70.
14. S. Bethke, J. Phys. G26 (2000) R27.
15. H1 Collab., C. Adloff et al., Eur. Phys. J. C19 (2001) 269.
16. ZEUS Collab., Measurement of High- Q^2 Neutral Current Cross Section in e^-p DIS and a First Measurement of the Structure Function xF_3 at HERA;
ZEUS Collab., Measurement of High- Q^2 Charged Current Cross Section in e^-p Deep Inelastic Scattering at HERA, contributed papers to ICHEP 2000, Osaka, Japan, July 2000.
17. H1 Collab., C. Adloff et al., Inclusive Measurement of Deep Inelastic Scattering at high Q^2 in Positron-Proton Collisions at HERA, contributed paper to ICHEP 2000, Osaka, Japan, July 2000.
18. CTEQ Collab., H.L. Lai et al., Phys. Rev. D55 (1997) 1280; hep-ph/9903282.
19. A.D. Martin et al., Eur. Phys. J. C4 (1998) 463; hep-ph/9803455 (1998).